Electronic structure of $MoSe_2$, MoS_2, and WSe_2. I. Band-structure calculations and photoelectron spectroscopy

R. Coehoorn,* C. Haas, J. Dijkstra, and C. J. F. Flipse
Laboratories of Physical and Inorganic Chemistry, Materials Science Centre of the University of Groningen, Nijenborgh 16, 9747 AG Groningen, The Netherlands

R. A. de Groot
Research Institute for Materials, Faculty of Science, University of Nijmegen, Toernooiveld, 6515 ED Nijmegen, The Netherlands

A. Wold
Department of Chemistry, Brown University, Providence, Rhode Island, 02918
(Received 20 October 1986)

The band structures of the semiconducting layered compounds $MoSe_2$, MoS_2, and WSe_2 have been calculated self-consistently with the augmented-spherical-wave method. Angle-resolved photoelectron spectroscopy of $MoSe_2$ using He I, He II, and Ne I radiation, and photon-energy-dependent normal-emission photoelectron spectroscopy using synchrotron radiation, show that the calculational results give a good description of the valence-band structure. At about 1 eV below the top of the valence band a dispersionless state was measured, almost completely of Mo $4d$ character. Such a state, which is not predicted by band-structure calculations, has also been observed in metallic layered compounds. Suggestions are given for the explanation of this phenomenon.

I. INTRODUCTION

The disulphides and diselenides of molybdenum and tungsten and the low-temperature phase of $MoTe_2$ (α-$MoTe_2$) form a class of semiconducting layered compounds with a trigonal prismatic coordination of the metal atoms. In the most common $2H$ polytype the hexagonal unit cell consists of two chalcogenide-metal-chalcogenide sandwich layers. Upon the $\alpha \rightarrow \beta$ phase transition at about 850 °C $MoTe_2$ becomes semimetallic. Like WTe_2, which is also semimetallic, β-$MoTe_2$ has a distorted octahedral coordination of the metal atoms.

The physical and structural properties of the transition-metal dichalcogenides have been reviewed extensively by Wilson and Yoffe.[1] The optical gaps range from about 1 eV for α-$MoTe_2$ to about 2 eV for WS_2. By a detailed analysis of his band-structure calculation of MoS_2, Mattheiss[2] showed that the semiconducting gap results from the combined effect of the ligand-field splitting and the d-d hybridization of Mo $4d$ states. Huisman *et al.*[3] showed that this ligand-field splitting of d levels in a trigonal prismatic coordination can be described better as an effect of metal-d—nonmetal-p covalency rather than as a crystal-field effect. The occupied part of the d band is often referred to as a d_{z^2} band, although it also contains a considerable amount of mixed Mo d_{xy}-$d_{x^2-y^2}$ character and, in particular at Γ, much S p_z character.[4] The splitting-off of this band, which contains two states per metal atom, stabilizes the trigonal coordination with respect to the octahedral coordination in compounds with a d^1 or d^2 configuration of the metal atom.[3] Band-structure calculations for MoS_2 (Refs. 2 and 4—8) situate this band (width about 1 eV) at the top of a 5—7-eV wide S $3p$—derived band, which contains a considerable amount of Mo d character because of strong covalent metal-nonmetal interactions. Band-structure calculations of the other compounds in the MoS_2 family have been performed only by Bromley *et al.*,[5] who did not take into account interlayer interactions. From their results, it can be concluded that the electronic structures of these compounds are very similar.

In the experimental work, too, MoS_2 was often regarded as the prototype for this class of compounds, as it is obtained easily as natural molybdenite. Optical-absorption and reflection spectra have been measured on all compounds in the MoS_2 family[1,9—12] On the basis of energy-dependent angle-integrated ultraviolet photoelectron spectroscopy (UPS), and a comparison of these results with x-ray absorption spectroscopy, optical-absorption and reflection spectroscopy, and electron-energy-loss spectroscopy, McMenamin and Spicer[13] constructed a model for the electronic structure of MoS_2. Important features of their model are a semiconducting band gap of at least 1 eV, a slight overlap of the Mo d_{z^2} and S p valence band and a valence-band maximum at Γ. As to these points the band-structure calculations[2,4—8] show no general agreement. Angle-resolved ultraviolet photoelectron spectroscopy (ARUPS) of MoS_2 and α-$MoTe_2$ has been performed by McGovern *et al.*[14,15] However, they were not able to interpret their results in terms of a band structure of these compounds. They attributed this difficulty to the complexity of the band structure and the photoemission process.

In this paper we present the results of self-consistent band-structure calculations of $MoSe_2$, MoS_2, and WSe_2, and photoelectron spectra of $MoSe_2$. The experimental band structure $E(\mathbf{k}_{||})$, measured with ARUPS using He I, He II, and Ne I radiation from a gas-discharge lamp, is

compared with a projection of the calculated band structure. The band structure $E(k_\perp)$ along the line ΓA in the Brillouin zone is derived from photon-energy-dependent measurements of the normal emission spectrum of $MoSe_2$, using synchrotron radiation with 18.5 eV $\leqq h\nu \leqq$ 60 eV. The theoretical and experimental band structures of $MoSe_2$ are in good agreement, and the calculated band structures of MoS_2 and WSe_2 are indeed very similar to that of $MoSe_2$, so therefore we have obtained a detailed picture of the electronic structure of the three compounds.

In Sec. II we give a description and the results of the band-structure calculations, and a brief discussion of effects of anion polarization on the calculated band structures. The photoelectron spectra, taken with radiation from a gas-discharge lamp in our own laboratory, are presented and compared with theory in Sec. III. An analysis of photoelectron spectra that were measured at the synchrotron laboratory in Daresbury (U.K.) is given in Sec. IV. Section V contains some concluding remarks. In a subsequent paper[16] the nature of the band gaps is discussed in more detail.

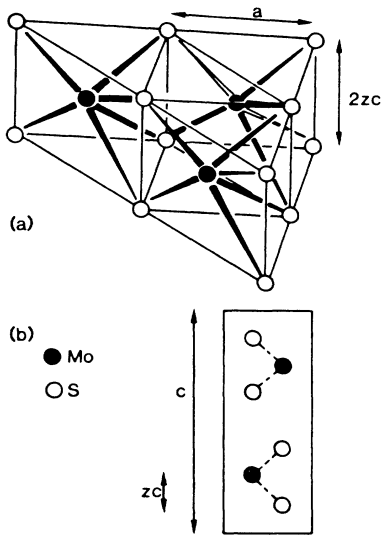

FIG. 1. (a) Part of a $MoSe_2$ sandwich layer, showing the trigonal prismatic coordination of the Mo atom. (b) (110) cross section of the hexagonal unit cell.

II. BAND-STRUCTURE CALCULATIONS

A. Computational method

Ab initio self-consistent band-structure calculations were performed using the augmented-spherical-wave (ASW) method.[17] The local-density approximation for exchange and correlation effects, as given by Hedin and Lundquist[18] was used. Scalar relativistic effects (mass velocity and Darwin terms) were included in the calculation.

$MoSe_2$, MoS_2, and WSe_2 crystallize in the hexagonal $2H_b$-MoS_2 structure with space group $P6_3/mmc$ D^4_{6h} (no. 194 in the *International Tables of Crystallography*). A part of a S-Mo-S sandwich layer, and the (110) cross section of the hexagonal unit cell are shown in Fig. 1. There are two equivalent Mo atoms at the $2c$ sites ($\pm\frac{1}{3}$, $\pm\frac{2}{3}$, $\pm\frac{1}{4}$) and four equivalent S atoms at the $4f$ sites ($\pm\frac{1}{3}$, $\pm\frac{2}{3}$, $\pm u$) and ($\pm\frac{2}{3}$, $\pm\frac{1}{3}$, $\pm(u+\frac{1}{2})$). The distance between metal and nonmetal layers is zc, with $z=\frac{3}{4}-u$, see Fig. 1.

Within the ASW method the crystal is subdivided into Wigner-Seitz spheres, centered around each atom, in which the potential is spherically symmetric. The difference between the real crystal potential and the ASW spherically symmetric atomic potentials is determined by the choice of the cation-to-anion atomic-radius ratio and by the possible inclusion of empty spheres at large interstitial sites. Calculations of $MoSe_2$ with different cation-to-anion atomic-radius ratios and with and without empty spheres at the ($2a$) sites (0,0,0) and (0,0,$\frac{1}{2}$) in the van der Waals gap showed differences up to 1 eV with respect to the relative band energies and widths. However, these differences did not affect our conclusions with respect to the positions of the direct and indirect gaps (see Ref. 16). In our final calculations the empty spheres were omitted. The Wigner-Seitz radii are given in Table I. The polarization of the nonmetal atom, which is an important factor

TABLE I. Input parameters for the ASW band-structure calculations.

		$MoSe_2$	MoS_2	WSe_2
Lattice constants[a]	a (Å)	3.288	3.1604	3.280
	c (Å)	12.900	12.295	12.950
	z	0.121	0.121	0.121
c/a ratio		3.924	3.89	3.948
Basis functions	Mo/W	5*s*,5*p*,4*d*	5*s*,5*p*,4*d*	6*s*,6*p*,5*d*
	S/Se	4*s*,4*p*,4*d*	3*s*,3*p*,3*d*	4*s*,4*p*,4*d*
Wigner-Seitz sphere radii (Å)				
	Mo/W	1.200	1.044	1.196
	S/Se	1.851	1.794	1.851

[a] Unit cell parameters a and c from F. Hulliger, *Structural Chemistry of Layer-Type Phases*, edited by F. Levy (Riedel, Dordrecht, 1976). The input parameter $z=0.121$ for the ASW calculations differs from the experimental value of $z=0.129$, in order to take account of polarization effects.

in the stabilization of layered structures,[19] is not taken into account self-consistently in the calculation of the potential. From a comparison of ARUPS spectra of some layered compounds with calculated ASW band structures, it was found that disregarding the polarization may lead to, for instance, a lower energy separation between the metal d and nonmetal p bands.[20] A decrease of the crystal parameter z (which corresponds to a decrease of the nonmetal-to-metal distance), was found to result in calculated band structures which show a much better agreement with ARUPS spectra. This decrease of the z parameter corresponds to a shift of the electrons of the nonmetal atoms in the direction of the nonmetal atoms (shell model of polarizability), and may be regarded therefore as a crude simulation of anion polarizability. In Sec. III it will be shown that for $MoSe_2$ a good agreement between theory and experiment can be obtained with $z=0.121$. The experimental value is $z=0.129$ for MoS_2,[21] $MoSe_2$,[22] and WSe_2.[23] The input parameters of the ASW calculations are given in Table I.

B. Results

Figures 2, 3, and 4 show the calculated band structures of $MoSe_2$, MoS_2, and WSe_2, respectively, along symmetry lines in the hexagonal Brillouin zone. For the symmetry labels we used the notation of Miller and Love.[24] Differences with the notation of Herring[25] were listed in Table III of Ref. 26. The top of the valence band at Γ is taken as the energy zero.

A quick insight into the character of the wave function of the bands can be obtained from the partial Mo and Se density of states (DOS), given for $MoSe_2$ in Fig. 5. The band at -14.8 eV to -12.4 eV is composed mainly of Se $4s$—derived states. At the top of the valence band there is the so-called d_{z^2} band (see Sec. I), from about -1.6 to 0 eV [Fig. 5(b)]. This band overlaps slightly with the higher binding-energy part of the valence band, which is predominantly of Se $4p$ character with covalently mixed- in Mo $4d$ character. The conduction band between 0.4 and 3.8 eV also shows considerable Mo $4d$—Se $4p$ covalency. The lower part of the conduction band is predominantly of Mo($4d$) character. Qualitatively the same conclusion holds for MoS_2 and WSe_2.

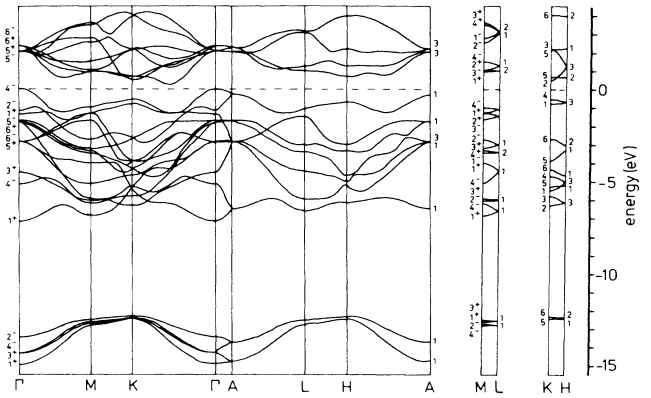

FIG. 3. Scalar relativistic band structure of $2H$-MoS_2.

For $MoSe_2$ the importance of spin-orbit interaction was estimated by treating it as a perturbation, using the self-consistent scalar-relativistic zero-order wave functions, by adding a term $\lambda \mathbf{L}\cdot\mathbf{S}$ to the Hamiltonian. This operator was taken to operate only on Se $4p$ states [with $\lambda=(\frac{2}{3})0.42$ eV] and Mo $4d$ states [with $\lambda=(\frac{2}{5})0.26$ eV], corresponding to atomic splittings of 0.42 and 0.26 eV, respectively.[27] The largest effect was found at Γ. There the twofold degenerate $\Gamma_5^-(-1.43$ eV) and $\Gamma_6^+(-1.49$ eV) states are split into states at -1.34, -1.40, -1.52, and -1.62 eV. The other states in the valence band at Γ, and the states at M and K, show shifts of 0.1 eV or less.

The calculated band structures indicate that the indirect gap originates from transitions from the top of the valence band at Γ to the bottom of the conduction band halfway between Γ and K. The direct optical gap is situated at the K point of the Brillouin zone. In a subsequent paper on the nature and magnitude of the semiconducting gaps we will show that these findings are consistent with optical-absorption and reflection data.[16] In this paper it will be shown from photoelectron spectroscopy that the calculated band structures give an accurate description of the electronic structure of the valence bands.

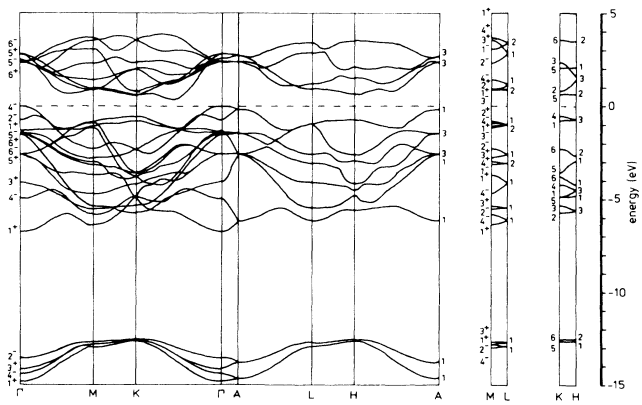

FIG. 2. Scalar relativistic band structure of $2H$-$MoSe_2$.

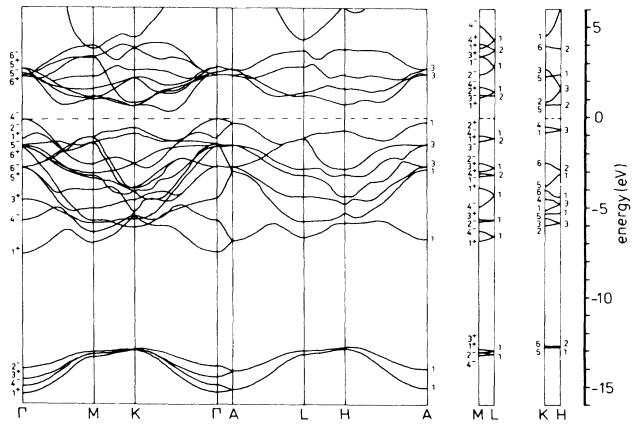

FIG. 4. Scalar relativistic band structure of $2H$-WSe_2.

III. PHOTOELECTRON SPECTRA—ANGULAR DEPENDENCE

Single crystals of $MoSe_2$ were grown by the vapor-transport technique, with Br_2 as the transport agent. The crystals were cleaved in the preparation chamber of a Vacuum Generators ADES 400 spectrometer, at a pressure of 10^{-7} Pa, and transferred quickly to the main chamber, where the base pressure was 10^{-8} Pa. In this section we give results obtained with a gas-discharge lamp, supplying unpolarized photons of 21.2 eV (He I), 40.8 eV (He II), and 16.8 eV (Ne I). The energy resolution, obtained with the hemispherical analyzer, was 0.1 eV, and the acceptance angle was $\pm 1°$. All spectra were taken with a light angle of incidence of $\alpha = 45°$.

In Figs. 6 and 7 we show the dependence of He I-ARUPS spectra on the polar angle θ, for emission in the ΓKHA and ΓMLA planes of the Brillouin zone, respectively. We also measured spectra at negative emission angles, up to $\theta = -30°$. The band structure is symmetric around $\theta = 0°$, but due to the different angle of the emitted electron with respect to the photon beam, the transition matrix elements are different. We observed indeed that the experimental band structure (peak positions as a function of $\mathbf{k}_{\|}$, the component of the wave vector parallel to the surface) was symmetric around $\theta = 0°$, but that the peak intensities were different. Since we will concentrate the discussion on the peak positions, the spectra at negative θ are not shown.

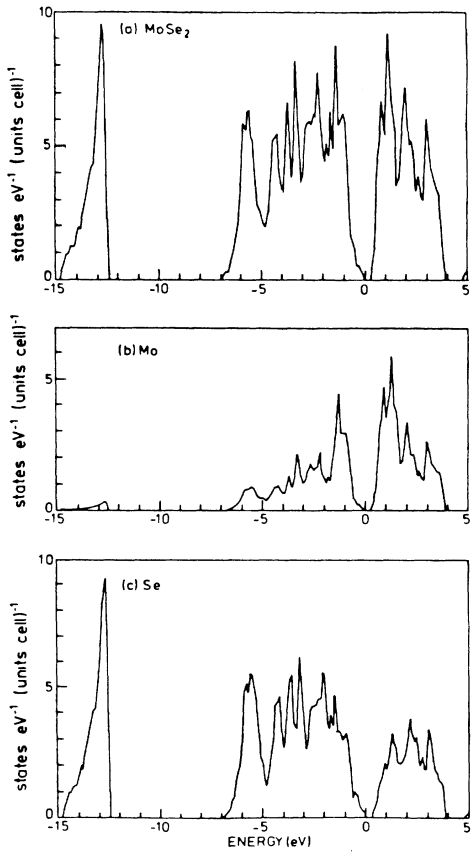

FIG. 5. (a) Total density of states of $2H$-$MoSe_2$. (b) Mo-partial density of states. (c) Se-partial density of states. Units: states eV^{-1} (unit cell)$^{-1}$. Scalar relativistic calculation without spin-orbit splitting.

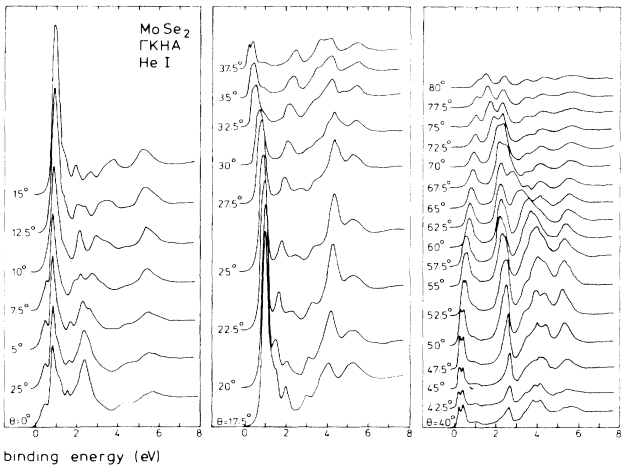

FIG. 6. He I ARUPS spectra of $MoSe_2$ with $\alpha = 45°$ at different angles θ in the ΓKHA plane.

In order to investigate the dependence of the spectra on the photon energy, ARUPS spectra of electrons emitted in the ΓKHA plane were also measured with He II and Ne I radiation. The He II spectra (Fig. 8) were measured with an analyzer energy resolution of 0.4 eV. The Ne I spectra were taken with a resolution of 0.1 eV in the interval $0° \leqq \theta \leqq 75°$. In Fig. 9 the normal-emission ($\theta = 0°$) spectrum is shown.

In Figs. 10 and 11 the peak positions from the He I spectra are compared with a projection of the calculated band structure of the surface Brillouin zone, for the ΓMLA and ΓKHA emission planes, respectively. He II and Ne I data for the KHA plane are shown in Figs. 12 and 13, respectively. Open circles are weak shoulders.

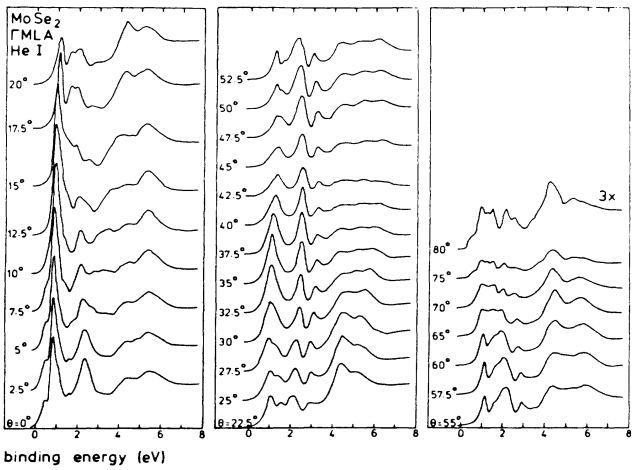

FIG. 7. He I ARUPS spectra of $MoSe_2$ with $\alpha = 45°$ at different angles θ in the ΓMLA plane.

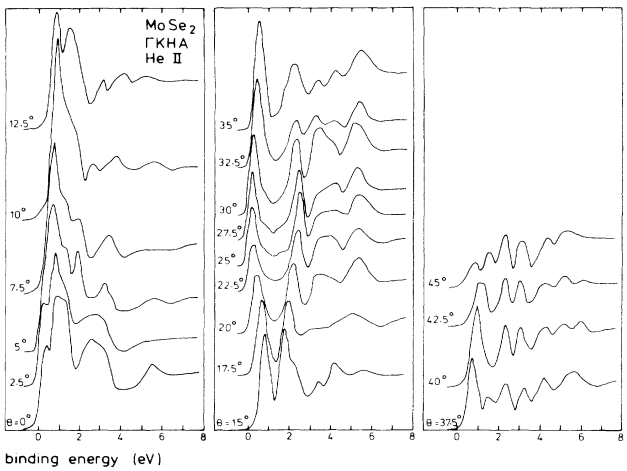

FIG. 8. He II ARUPS spectra of $MoSe_2$ with $\alpha=45°$ at different angles θ in the ΓKHA plane.

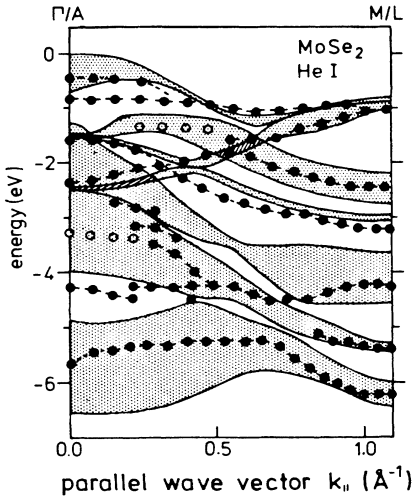

FIG. 10. Comparison of experimental and theoretical band structure of $MoSe_2$. ΓMLA emission plane. He I radiation.

From these figures it can be seen that an assignment of most of the peaks to the calculated bands is possible. For the six lower bands (in fact 12 bands which are pairwise connected at the ALH top face of the Brillouin zone) there is a good general agreement with respect to their energy position and dispersion. There are some minor disagreements, e.g., with respect to the calculated band at about -2.3 at K/H, which should be shifted downward by about 0.2 eV.

The agreement of theory and experiment with respect to the two upper bands at ML shows that the position of the "d_{z^2} band" with respect to the Se p—derived bands is described correctly by theory. The calculated dispersion of this band, however, is in disagreement with experiment, most clearly at K/H. Here two peaks were measured, approximately 0.3 eV above the calculated position. The distance between the peaks is 0.21 ± 0.02 eV, as determined with He I and Ne I radiation using an improved analyzer resolution of 0.02 eV.[16] The calculated energy distance between the corresponding K_1 and K_4 states is 0.33 eV (including spin-orbit interaction).

Another point of disagreement at the top of the valence band is the occurrence of a rather dispersionless peak at about -1 eV, which is clearly present in the ΓKHA and ΓMLA spectra near Γ/A, but which is also observed in the ΓKHA spectra near K/H as a weak shoulder. Normal-emission synchrotron spectra show that its peak position is photon energy independent, and that it is predominantly of Mo $4d$ character (Sec. IV). Such a dispersionless peak near the energy position of the metal d band was also seen in spectra of $TiTe_2$,[28] VSe_2,[29] $NbSe_2$,[30] $1T$-TaS_2, $1T$-$TaSe_2$ and $2H$-$TaSe_2$.[31] De Boer *et al.*[28] suggested that this peak is due to emission from a localized polaronic state. If an electron is emitted from a state in a polaron band, the polarization cloud left behind corresponds to a wave packet consisting of states with various **k** vectors. As the total wave vector **k** of the polaron

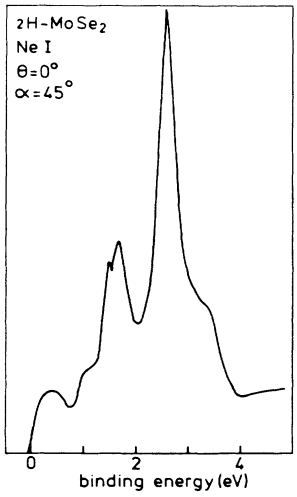

FIG. 9. Ne I ARUPS spectrum of $MoSe_2$ with $\alpha=45°$ at $\theta=0°$.

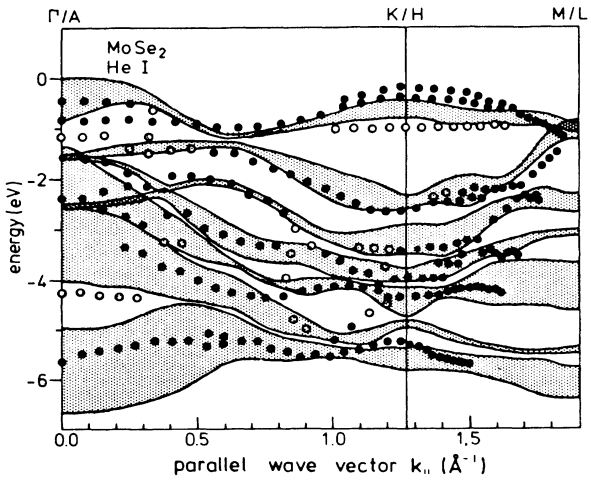

FIG. 11. Comparison of experimental and theoretical band structure of $MoSe_2$. ΓKHA emission plane. He I radiation.

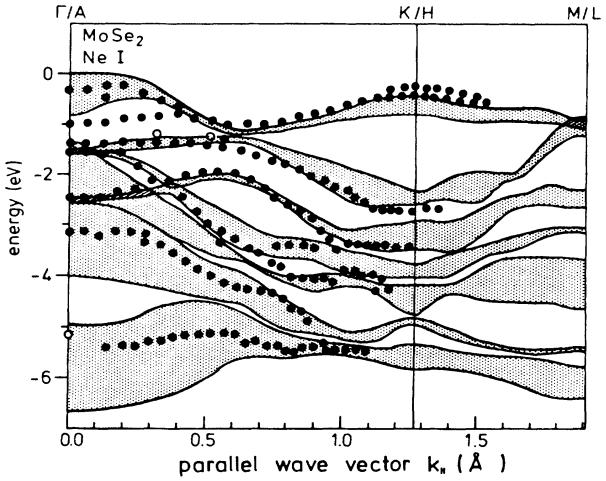

FIG. 12. Comparison of experimental and theoretical band structure of $MoSe_2$. ΓKHA emission plane. He II radiation.

is a good quantum number, this implies that the emitted electron can have an arbitrary **k**, leading to a dispersionless peak. Here we have found for the first time such a dispersionless peak in a semiconductor. This finding is important in the discussion on the nature of the interaction which produces the localization of the *d* electrons. One of the suggested explanations for the dispersionless state is that of an electronic polaron, with localization of the *d* electron due to polarization as a result of small-energy excitations across the Fermi level. This explanation can be valid in metallic crystals such as $TiTe_2$, but not in semiconductors as $MoSe_2$. Another possibility is localization due to interaction with the lattice (vibronic polaron). Alternative explanations are the occurrence of self-intercalation (Mo atoms in the van der Waals gap, leaving vacancies at their regular sites), or the occurrence of surface states. These explanations fit into the observation that, due to its Mo 4*d* character, the dispersionless state is an intrinsic property of the material, and that therefore it is not due to impurities in the bulk or at the surface. However, appreciable self-intercalation is not very likely in $MoSe_2$, since the crystals cleave very easily, indicating weak interlayer interactions.

A manifestation of spin-orbit splitting is observed in the normal emission Ne I spectrum (Fig. 9) at -1.5 eV. The distance between the peaks is 0.2 eV, equal to the calculated centers of the spin-orbit split bands at -1.37 and -1.57 eV (Sec. II). The calculated splitting of 0.1 eV between the Γ_6^- and Γ_5^+ bands at -2.5 eV is not resolved in the spectra.

IV. PHOTOELECTRON SPECTRA—PHOTON-ENERGY DEPENDENCE

In this section we present and discuss photon-energy-dependence ARUPS spectra of $MoSe_2$, measured with synchrotron radiation at Daresbury, England. From these spectra we have derived the band dispersion along ΓA, and the wave-function character of the dispersionless state at about -1 eV. The measurements were performed on an ADES-400 spectrometer, which is essentially identical to the apparatus in our home laboratory (Sec. III). The angular resolution was $\pm 2°$.

In Fig. 14, normal-emission spectra are shown in the photon-energy interval $18.5\ \text{eV} \leqq h\nu \leqq 60\ \text{eV}$. The light angle of incidence was $\alpha = 45°$. The monochromator resolution and the analyzer resolution were both equal to 0.2 eV, yielding a total resolution of 0.28 eV.

The photon-energy dependence of the peak positions can be analyzed within the direct transition model (three-step model). The positions of the critical points of the final-state bands can be derived from the dispersion of the bonding p_z band (4.9—6.7 eV binding energy), the antibonding p_z band (2.3—4.0 eV binding energy) and the d_{z^2} band (just below the top of the valence band). There are critical points at ~ 16, 20, 32, and 45 eV above the top of the valence band. In Fig. 15(a) we have connected the three upper critical points by a free-electron band with the energy zero at 12-eV binding energy. The final-state wave

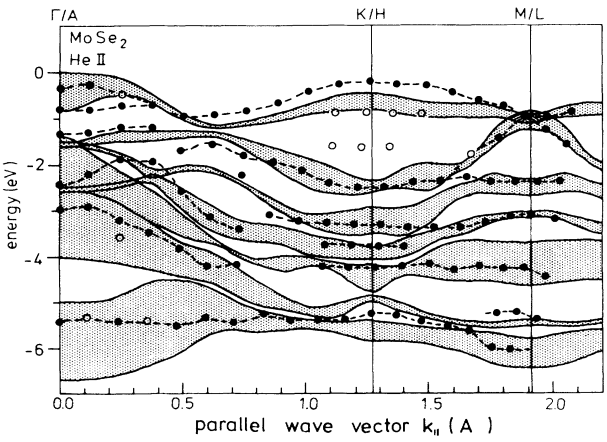

FIG. 13. Comparison of experimental and theoretical band structure of $MoSe_2$. ΓKHA emission plane. Ne I radiation.

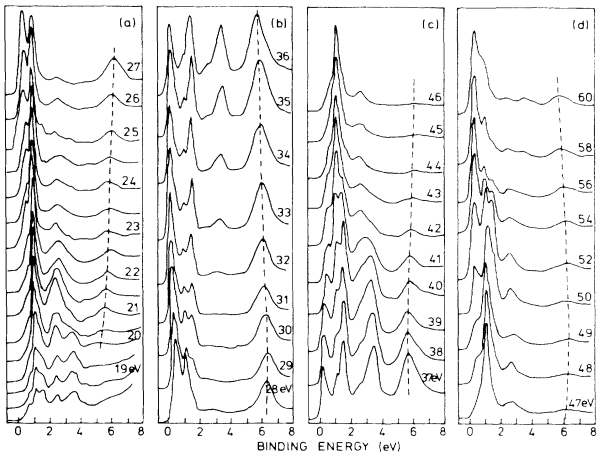

FIG. 14. Normal emission ARUPS spectra of $MoSe_2$, with $\alpha = 45°$, in the photon-energy range $18.5\ \text{eV} \leqq h\nu \leqq 60\ \text{eV}$.

functions are plane waves that propagate normal to the surface. The normal component $k_{\perp i}$ of the wave vector of the photoelectron in the initial state is assumed, within the direct transition model, to be equal to $k_{\perp f}$, which follows easily from the assumed final-state dispersion relation $E(k_{\perp f})$. In our analysis we also have to include the transition probabilities from initial to final states. At Γ, the final states are degenerate pairs with Γ_1^+ and Γ_2^-, or Γ_3^+ and Γ_4^- symmetry. From the dipole selection rules

$$\Gamma_1^+ \leftrightarrow \Gamma_2^- \quad \text{and} \quad \Gamma_3^+ \leftrightarrow \Gamma_4^-$$

with z polarized light, and

$$\Gamma_6^+ \leftrightarrow \Gamma_2^-, \quad \Gamma_6^- \leftrightarrow \Gamma_1^+, \Gamma_5^+ \leftrightarrow \Gamma_4^-, \quad \text{and} \quad \Gamma_5^- \leftrightarrow \Gamma_3^+$$

with x,y polarized light, it follows that electrons in each initial state can be excited to either a Γ_1^+ or Γ_2^- state, or to a Γ_3^+ or Γ_4^- state. These matrix element effects can be expressed conveniently by drawing the bands in a double Brillouin zone, with only those bands between which (strong) transitions are possible [Fig. 15(b)]. Here it has been assumed that away from Γ, along A, the rules are still quite effective, although they are less strict. Note that we now analyze the situation as if a $MoSe_2$-unit cell consists of one sandwich layer. Figure 15(c) shows the experimental band structure (dots) and the theoretical one (lines) along A. The agreement is quite good, apart from a dispersionless band at about 1-eV binding energy. These peaks were also observed in the He I and Ne I spectra. Another notable point is that the dispersion within the bonding p_z band is much smaller than calculated.

The photon-energy dependence of the peak intensities gives information about the atomic character of the initial states. The Mo $4d$ cross section exhibits a resonant behavior at $h\nu \approx 41$ eV due to interference with $4p$-$4d$ Coster-Kronig Auger decay. The spin-orbit split Mo $4p$ core levels have binding energies of 35.9 and 39.8 eV. At $h\nu = 38$ eV the Mo $4d$ cross section is low, and the spectra

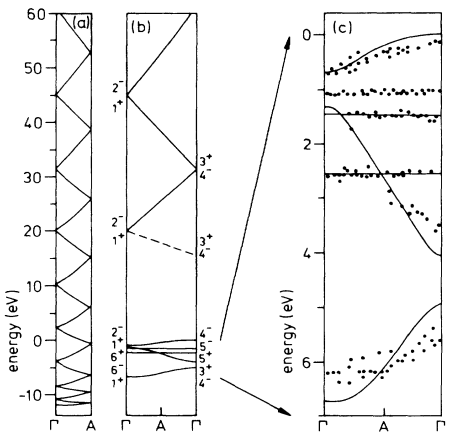

FIG. 15. (a) Free electron band structure along ΓA. Only plane waves that propagate normal to the surface are included. (b) Initial and final states for normal emission from $MoSe_2$. As discussed in the text the Brillouin zone is doubled in order to take matrix element effects into account. (c) Experimental (dots) and theoretical (lines) band structure of $MoSe_2$, along ΓA.

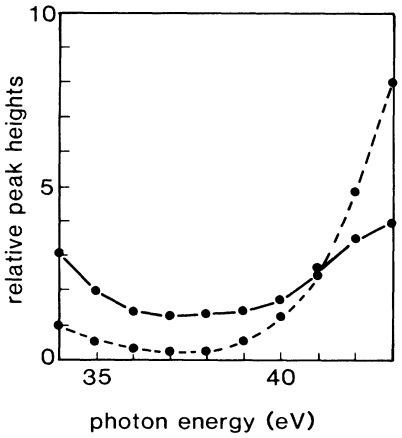

FIG. 16. Peak height of the dispersionless peaks at -1 eV, — — —, and -1.5 eV, ——. The figure shows the effect of the $4p$-$4d$ resonance on the Mo $4d$ cross section.

are dominated by peaks from states with much Se $4p$ character. In Fig. 16 we show the height of the dispersionless peaks at about -1 and -1.5 eV, as a function of the photon energy. The heights are relative to the height of the peak at about -3.5 eV, which is due to excitations from states close to the Γ_3^+ state. Owing to its symmetry this state does not have Mo $4d$ character. According to the band-structure calculations, the states from which the -1.5-eV peak originates (at Γ with Γ_5^- and Γ_6^+ symmetry) contain 67% Mo d character. The much more pronounced resonant behavior of the -1-eV peak indicates that these states contain even more d character. In Sec. III we have already used this observation as an important piece of information in our discussion of the origin of the -1-eV dispersionless state.

V. CONCLUSIONS

From angle-resolved photoelectron spectroscopy it was shown that the band structure of the occupied states of $MoSe_2$ is described very well by the calculated ASW band structure. The calculated band structures of MoS_2 and WSe_2 are very similar and, because of the good agreement with experiment in the case of $MoSe_2$, the results of the calculations for these compounds too are expected to be reliable. The photon-energy dependence of the normal-emission photoelectron spectra can be analyzed within the direct transition model if dipole selection rules are taken into account. An interesting result of the photoelectron spectroscopy experiments is the discovery of a dispersionless state at about -1 eV below the top of the valence band, consisting almost completely of Mo $4d$ character. Such a state, which cannot be explained from the band structure, was also observed in some metallic layered compounds. However, this is the first observation of such a state in a semiconducting compound. Possible explanations for the state are excitation from a polaronic state, the occurrence of self-intercalation or excitations from surface states.

Finally, the calculations and experiments give useful in-

formation about the nature of the semiconducting gaps, as discussed in detail in a subsequent paper.[16]

ACKNOWLEDGMENTS

We would like to thank D. Norman and D. Law for their help with the photoelectron spectroscopy experiments at the Synchrotron Radiation Source at Daresbury (U.K.). This investigation was supported by the Netherlands Foundation for Chemical Research [Scheikundig Onderzoek Nederland (SON)] with financial aid from the Netherlands Organization for the Advancement of Pure Research [Nederlandse Organisatie voor Zuiver-Wetenschappelijk Onderzoek (ZWO)], in conjunction with the collaborative agreement between ZWO and the United Kingdom Science and Engineering Research Council on the use of synchrotron radiation.

*Present address: Philips Research Laboratories, P.O. Box 80.000, 5600 JA Eindhoven, The Netherlands.

[1]J. A. Wilson and A. D. Yoffe, Adv. Phys. **18**, 193 (1969).
[2]L. F. Mattheiss, Phys. Rev. Lett. **30**, 784 (1973); Phys. Rev. B **8**, 3719 (1973).
[3]R. Huisman, R. de Jonge, C. Haas, and F. Jellinek, J. Solid State Chem. **3**, 56 (1971).
[4]D. W. Bullett, J. Phys. C **11**, 4501 (1978).
[5]R. A. Bromley, R. B. Murray, and A. D. Yoffe, J. Phys. C **5**, 759 (1972).
[6]R. V. Kasowsky, Phys. Rev. Lett. **30**, 1175 (1973).
[7]K. Wood and J. B. Pendry, Phys. Rev. Lett. **31**, 1400 (1973).
[8]S. P. Hind and P. M. Lee, J. Phys. C **13**, 349 (1980).
[9]A. R. Beal and H. P. Hughes, J. Phys. C **12**, 881 (1979).
[10]A. R. Beal, W. Y. Liang, and H. P. Hughes, J. Phys. C **9**, 2449 (1976).
[11]Kam-Keung Kam, Chi-Lan Chang, and D. W. Lynch, J. Phys. C **17**, 4031 (1984).
[12]P. M. Amirtharaj, F. M. Pollak, and A. Wold, Solid State Commun. **41**, 581 (1982).
[13]J. C. McMenanim and W. E. Spicer, Phys. Rev. B **16**, 5474 (1977).
[14]I. T. McGovern, K. P. Childs, H. M. Clearfield, and R. H. Williams, J. Phys. C **14**, L243 (1981).
[15]I. T. McGovern, R. H. Williams, and A. W. Parke, J. Phys. C **12**, 2684 (1979).
[16]R. Coehoorn, C. Haas, and R. A. de Groot, following paper, Phys. Rev. B **35**, 6203 (1987).
[17]A. R. Williams, J. Kübler, and G. D. Gelatt, Jr., Phys. Rev. B **19**, 6094 (1979).
[18]L. Hedin and B. I. Lundquist, J. Phys. C **4**, 2064 (1971).
[19]C. Haas, in *Physics of Intercalation Compounds*, edited by L. Pietronero and E. Tosatti (Springer-Verlag, Berlin, 1981), p. 158.
[20]R. Coehoorn, A. A. van Heuzen, C. Haas, and G. A. Sawatzky, in *Festkörperprobleme-Advances in Solid State Physics*, edited by P. Grosse (Vieweg, Braunschweig, 1985), Vol. XXV, p. 459.
[21]R. G. Dickinson and L. Pauling, J. Am. Chem. Soc. **45**, 1466 (1923).
[22]K. D. Bronsema, J. L. de Boer, and F. Jellinek, Z. Anorg. Alg. Chem. **540/541**, 15 (1986).
[23]W. Schutte and J. L. de Boer (unpublished).
[24]S. C. Miller and W. F. Love, *Tables of Irreducible Representations of Space Groups and Corepresentations of Magnetic Space Groups* (Pruett, Boulder, 1967).
[25]C. Herring, J. Franklin Inst. **233**, 525 (1942).
[26]R. Coehoorn, C. Haas, and R. A. de Groot, Phys. Rev. B **31**, 1980 (1985).
[27]F. Herman and S. Skillmann, *Atomic Structure Calculations* (Prentice-Hall, Englewood Cliffs, N.J., 1963).
[28]D. K. G. de Boer, C. F. van Bruggen, G. W. Bus, R. Coehoorn, C. Haas, G. A. Sawatzky, H. W. Myron, D. Norman, and H. Padmore, Phys. Rev. B **29**, 6797 (1984).
[29]H. P. Hughes, C. Webb, and P. M. Williams, J. Phys. C **13**, 1125 (1980).
[30]F. Minami, M. Sekita, N. Aono, and N. Tsuda, Solid State Commun. **29**, 459 (1979).
[31]N. V. Smith and M. M. Traum, Phys. Rev. B **11**, 2087 (1975).